Nanoscale

PAPER

View Article Online
View Journal | View Issue

Cite this: *Nanoscale*, 2023, **15**, 19314

Evidence for an L_3 phase in ternary deep eutectics: composition-induced L_3-to-L_α transition of AOT†

Oliver S. Hammond, *‡[a] Naomi S. Elstone, §[a] James Doutch,[b] Peixun Li [b] and Karen J. Edler [a,c]

Received 27th July 2023,
Accepted 17th November 2023

DOI: 10.1039/d3nr03689h

rsc.li/nanoscale

Pure and hydrated deep eutectic solvents (DES) are proposed to form self-assembled nanostructures within the fluid bulk, similar to the bicontinuous L_3 phase common for ionic liquids (ILs). Labelled choline chloride : urea : water DES were measured using small-angle neutron scattering (SANS), showing no long-range nanostructure. However, solutions of the surfactant AOT in this DES yielded scattering consistent with the L_3 "sponge" phase, which was fitted using the Teubner–Strey model. A disclike model gave local structural information, namely, a linear increase in radius *versus* solvent water content (*w* = molar ratio of DES : water), eventually forming large, turbid lamellar phases at 10*w*; an L_3-to-L_α transition was observed. Simultaneous multi-contrast SANS fits show the surfactant headgroup region is dominated by interactions with poorly-soluble Na^+ at low water contents, and numerically-superior $[cholinium]^+$ as water content increases. The modified interfacial Gaussian curvature from cation : anion volume matching stabilizes the lamellar morphology, allowing the bilayer aggregation number to increase.

Introduction

Exerting fine control over the separation of polar and non-polar phases is an ongoing challenge to chemical science of enormous economic pertinence. Colloid science offers several solutions to this: the most common is through (micro- or nano-) emulsions, facilitated by interfacial self-assembly of amphiphilic surfactant molecules, to achieve a phase with either long-term kinetic, or true thermodynamic stability, containing separated hydrophobic and hydrophilic domains.[1] More recently, stable phase segregation was shown to exist on the intermolecular scale, such as upon addition of an amphiphilic co-solvent even as small as methanol to water.[2] Pronounced L_3-type spongelike nanostructure was first observed in surfactant systems,[3–5] and has since been reported within the solvent bulk itself, particularly for ionic liquids (ILs),[6] which can be 'designed' as concentrated amphiphilic salt melts, by selection of chemical moieties to 'switch' structuring on or off.[7–9] These different phase separation methodologies are crucial for industry and society, for example in hydrocarbon recovery, chemical synthesis microreactors, templating of nanostructured functional materials, and delivery of active pharmaceutical ingredients (APIs). This is because controlled phase separation enables specific solute–solvent interactions, and hence the desired level of activity for the solute in question.[10,11]

Deep Eutectic Solvents (DES) are a subclass of eutectic mixtures,[12] where enthalpic and entropic contributions reduce the melting point relative to that of the corresponding ideal mixture.[13,14] DES can be related to ionic liquids (ILs), in terms of ionic strength, ion pairing, clustering, and nanostructure,[15–17] but the validity of any comparison depends upon the chemical composition and mixing ratio.[18,19] DES have a Debye length longer than expected for concentrated electrolytes, as charge propagates more easily through correlated ions.[20,21] These benefits have been leveraged in deployment as 'green' and 'designer' drop-in replacements for conventional hazardous solvents, in applications including chemical synthesis,[22] electrodeposition,[23] and nanomaterial manufacturing.[24] Despite their ionic character, DES were recently shown to support the self-assembly of a variety of anionic, cationic, zwitterionic, and non-ionic amphiphiles.[25–28] Excitingly, DES composition allows for tailoring of micelle morphology, *via* solvent–counterion and surfactant–solvent interactions which alter the effective surfactant headgroup size, defining the packing.[29,30] A fertile strategy has been the controlled dosing of DES with

[a]*Centre for Sustainable Chemical Technologies & Department of Chemistry, University of Bath, Claverton Down, Bath BA2 7AY, UK. E-mail: oliver.s.hammond@bath.edu*
[b]*ISIS Neutron & Muon Source, Science and Technology Facilities Council, Rutherford Appleton Laboratory, Harwell-Oxford OX11 0QX, UK*
[c]*Centre for Analysis and Synthesis, Department of Chemistry, Lund University, Lund 221 00, Sweden*

†Electronic supplementary information (ESI) available: Experimental procedures, data analysis, and fitting parameters. See DOI: https://doi.org/10.1039/d3nr03689h

‡Current address: Department of Biological and Chemical Engineering, Aarhus University, Aarhus C 8000, Denmark.
§Current address: Department of Chemistry, University of York, Heslington yo10 5DD, UK.

water:[31] below a systemic threshold, the DES structural characteristics are maintained,[17] but viscosity, cost and sustainability are improved,[32] forming a low-melting ternary eutectic system.[31,33] The improvement in transport properties is particularly pertinent, allowing for more rapid dissolution of solutes.[11] Despite this promise, structural understanding lags behind application-driven studies, inhibiting informed progress.[34] In particular, nanostructures have been proposed for hydrophilic DES such as ChCl–urea (and aqueous mixtures thereof) from indirect inferences such as NMR spectroscopy,[35] but no direct evidence has been provided for the formation of the anomalous spongelike L_3 phases, whereas these are relatively common structures in amphiphilic ILs.[36] McDonald *et al.* have shown small-angle nanostructure in binary DES engineered to contain long alkyl subunits,[37] which has recently also been shown for choline chloride : butyric acid DES.[38] However, the question of nanostructure in archetypal, non-amphiphilic DES such as ChCl–urea, remains open and debated, and the same is true for ternary DES;[39] this issue is therefore important to resolve considering the popularity of these systems. Since ChCl–urea is the most widely used DES in studies of amphiphile self-assembly, we have chosen this system as a model starting point towards myriad future studies, expanding on the possibilities of solute organisation in such solvents.

Dioctyl sodium sulfosuccinate (*aka*. AOT, DOSS, or docusate) is an anionic amphiphile, with iconic dual branched (diethylhexyl) tails.[40] The 'wedgelike' molecular geometry of AOT defines its self-assembly properties,[41] thus it is commonly found at the liquid–liquid interface in emulsion formulations,[42] and is the prototypical reverse micelle-former in oils.[43] Due to this interesting phase behaviour,[44,45] it has been deployed in a wide variety of applications such as the dispersal of oil spills, reduction of crop pests, and treatments for constipation.[46] AOT has been shown to display surface activity in the classic ChCl–urea DES, including in the presence of water. Critical micelle concentrations (CMCs) and surface tension reductions due to saturation of the air–DES interface have been measured, relatable to those for AOT in traditional molecular solvents.[47] DES–surfactant systems lack quality structural data, such that micellization therein is not properly understood. Here, we therefore present results from small-angle neutron scattering (SANS) experiments with contrast variation – a direct, non-destructive diffraction method for probing the structure of DES and AOT micelles.[48] For mixtures containing AOT above the reported CMC values, with a DES composition of $X_{ChCl} = 0.33$ and $X_{Urea} = 0.67$, and under systematic variation of the DES : water molar ratio (w) from 0–10, we show the origin of observed nanostructure is entirely from AOT. The self-assembled morphology undergoes a phase transition from L_3 to L_α, which we can control *via* the solvent composition.

Results

Solvent backgrounds with different isotopic substitutions were first measured (Fig. 1). These datasets allowed us to test whether any measured small-angle scattering may derive from amphiphilic nanoscale heterogeneity (nanostructure) in the solvent itself. None of our SANS data show evidence for solvent nanostructure, across the entire small-angle region, or at any water content. This is particularly important for the d_9-choline chloride- : d_4-urea : H_2O (D : D : H) contrast set (Fig. 1d), which has the largest difference between the neutron scattering length densities for the DES and water (ΔSLD), chosen to highlight water pockets. These SANS data allow us to confirm that no DES–water structuring is observed across a real space distance range of *ca.* 0.6–60 nm, and thus, there is no spongelike L_3 nanostructure corresponding with an aqueous nanophase. At high-Q, the data deviate from the flat background, aligning perfectly with the 'solvent structure' pre-peaks reported previously using wide-Q-range neutron diffraction.[17] Similarly, there is no latent, broad small-angle scattering structure, as has been observed for liquids containing small nanosegregated regions, which is common in ILs,[49,50] and has also been seen in systems which are conventionally considered as homo-

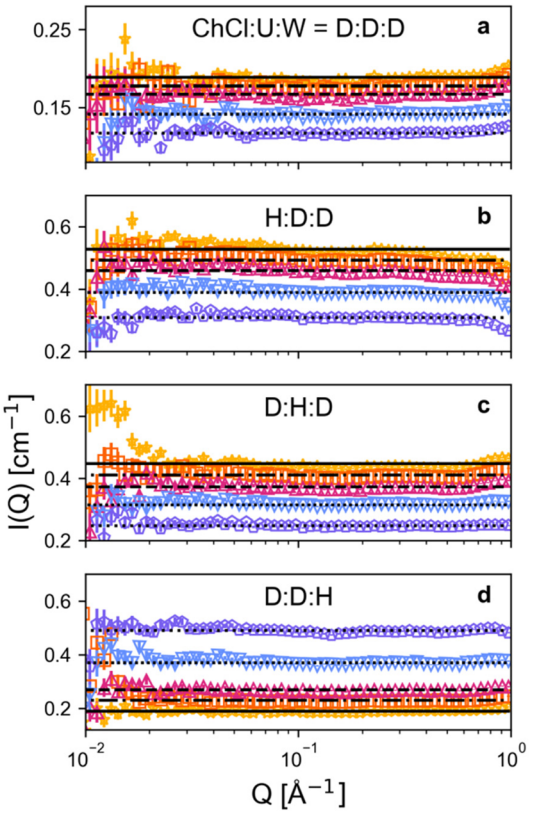

Fig. 1 Small-angle neutron scattering (SANS) data of pure solvents with choline chloride : urea : water contrasts of D : D : D (a), H : D : D (b), D : H : D (c), and D : D : H (d) following subtraction of the instrumental background. Water contents (in mole equivalents) are shown as yellow stars (0w), orange squares (1w), red upwards triangles (2w), blue downwards triangles (5w) and purple pentagons (10w). Lines (solid = 0w, dot-dashed = 1w, dashed = 2w, finely dotted = 5w, loosely dotted = 10w), corresponding with flat backgrounds set to the median measured I(Q) value for each water content dataset, are plotted as a guide.

geneous, such as tetradecane, where a radius of gyration (R_g) can be elucidated by isotopic labelling of H-tetradecane : d_{30}-tetradecane mixtures.[51] The only other signal observed was an experimental artefact at *ca.* 0.015 $Å^{-1}$ for some 0*w* samples, which we assign to the short collection time, which causes issues because of the intrinsically low signal : noise ratio at low-Q on this instrument; this is seen in several measurements. The low-Q artefact is most profound in the D : H : D contrast, so the improbable alternative explanation would be large (*ca.* 40 nm) urea clusters in the pure DES.

Following background subtraction, several models were initially trialled (see comparison in Fig. S1†), to determine the best fit to the SANS data while minimising over-fitting, sources of error and biases. We generally favoured the models with the fewest possible fitted variables. For samples where $w \leq 5$, fitting was possible using the Teubner–Strey microemulsion model (Fig. S2†) which is known to be a good fit for L_3-type systems, but data could also reliably fitted to an oblate ellipsoid model with modified Percus-Yevick hard sphere structure factor (S(Q); accounting for excluded volume effects), which has previously also been used to represent the L_3 phase, and offers a more detailed local structural picture.[30,52] Despite the changing morphology, the choice of a hard sphere structure factor was kept constant here to facilitate comparison, particularly as data on the dielectric constant in ternary DES as a function of composition is currently lacking. For the most hydrated (10*w*) systems, the ellipsoid model was only a valid descriptor at the highest AOT concentration, 5 wt%. The 1 wt% and 2 wt% AOT samples in 10*w* DES fitted best to a uniform lamellar sheet whose equatorial radius (R_{eq}) exceeds the instrumental resolution; the S(Q) was removed for the lamellar model.

The full set of data, fitted either to oblate ellipsoids with a hard sphere S(Q), or to a lamellar sheet model for the samples containing 1 wt% and 2 wt% of AOT in the 10*w* DES, is therefore shown in Fig. 2. The calculation of SLDs is provided in Table S1,† and the accompanying fitted parameters for all datasets are provided in Tables S2–S4.† As can be seen, the models generally fit very well, but some discrepancies occur in the fitted radii, scale factor or volume fractions, which can be attributed to the varied sources of experimental error which includes chemical differences between isotopologues (*i.e.* concentration and nature of impurities), transmission and background corrections, and variable contrast within each sample series, as water content varies (refer to Fig. 1 to see the inherent scattering background level fluctuation). Moreover, certain samples represent edge cases in terms of our chosen model and instrument configuration, such as the 5*w* samples, where the S(Q) starts to fall off, the turnover in the low-Q signal approaches the low-Q instrumental limit, and the micelles are functionally almost lamellar at this point.

The Teubner–Strey model is a shape-independent function used to fit microemulsion-like systems, and is parameterized in terms of periodicity (d-spacing), correlation length ξ, and volume fraction ϕ.[53,54] The L_3 sponge phase swells with addition of solvent, and thus is characterised by a linear dependence between d-spacing and $\phi_{solvent}$, which we observed for samples with $w \leq 2$, as is shown in Fig. 3a.[55] From the other described fitting method, the calculated trends in micelle morphology are shown in Fig. 3b–f as a function of the molar ratio of water in the DES (w). The polar radius (R_{po}; disc thickness) of the micelle remains almost constant as water is added. Since our available solvent–surfactant contrasts should predominantly highlight the hydrophobic alkyl tail domain, this implies insignificant penetration into the micelle core by the DES mixture. Conversely, most other fitted (linked) micelle parameters; equatorial radius (R_{eq}; disc width), aggregation number, and aspect ratio, increase linearly as further water is introduced. Therefore, at low water content (*i.e.*, pure DES with high ionic strength), the AOT micelles form discs of *ca.* 2 nm thickness and 12 nm diameter, and increasing the water content (thereby reducing the ionic strength of the solution by dilution) rapidly increases the micelle disc diameter, reaching *ca.* 30 nm at 5*w*, and generally exceeding the instrument resolution to appear as full lamellar sheets at 10*w*, except for the highest AOT concentration. The noteworthy exception to the linear increase in fitted parameters as a function of water content is $\phi_{S(Q)}$, *i.e.* the volume fraction of hard spheres; this parameter decreases linearly with increased water content in these systems.

For the most ideally-scattering sample set (1 wt% AOT, 0*w*), it was possible to co-refine a platelike core–shell cylinder model with Percus-Yevick hard sphere S(Q) to resolve the micellar fine structure (see Fig. 4). The shell SLDs were allowed to vary freely; this gave a plate radius of 50.1 ± 3.5 Å, outer shell thickness of 4.1 ± 3.5 Å, and inner core radius of 13.0 ± 3.9 Å, commensurate with the expected tail length and head thickness for AOT micelles.[56] The shell composition was subsequently modelled through least-squares fits of the DES component and AOT headgroup mole fractions to the calculated shell SLD values (see Table S5†), using the determined component SLDs. SLD calculations assumed a headgroup of $-(CO_2)_2CH_2CHSO_3Na$, but due to the similar scattering lengths, including Na^+ here does not have a major effect on the headgroup SLD. From this analysis, the micelle shell composition was calculated to be $x_{ChCl} = 0.035 \pm 0.012$, $x_{Urea} = 0.153 \pm 0.093$, $x_{AOTHead} = 0.812 \pm 0.080$. Therefore, in the pure DES, choline appears to be mostly excluded, and urea penetrates to a small fraction, as previously seen for sodium dodecylsulfate in choline chloride : urea : glycerol solvents.[29] There is some precedent for preferential AOT–urea interactions, such as those seen in urea clusters within AOT reverse micelles, where it is the most favourable solvation configuration in a hydrophobic environment.[57] It was not possible to co-refine all datasets in this manner. Our structural data therefore suggests that, at low water content, the AOT headgroups interact preferentially with urea, which also suggests that Na^+ ions have relatively low solubility in the DES bulk, and the surfactant headgroups are screened predominantly by Na^+, rather than Ch^+, despite the significant molar excess of the latter.

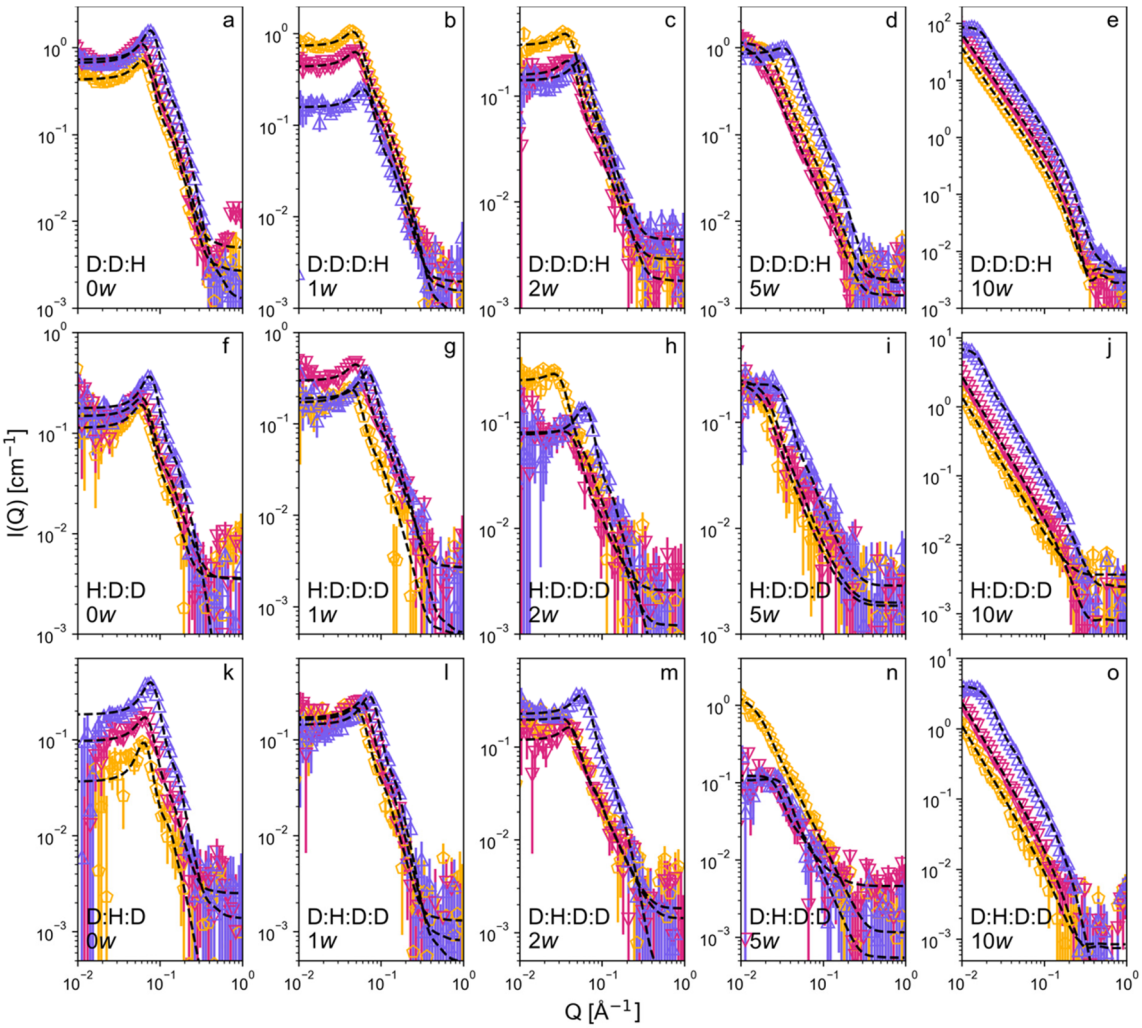

Fig. 2 Small-angle neutron scattering (SANS) data of samples containing H-AOT, D-choline chloride, D-urea, and D_2O (a–e; row 1), D-AOT, H-choline chloride, D-urea and D_2O (f–j; row 2), D-AOT, D-choline chloride, H-urea and D_2O (k–o; row 3). Fits are shown as dashed black lines, while measurements are shown as yellow pentagons (1 wt% AOT), red downwards triangles (2 wt% AOT) and purple upwards triangles (5 wt% AOT), and datasets are subdivided into anhydrous samples (a, f and k; column 1), and those containing 1 (b, g and l; column 2), 2 (c, h and m; column 3), 5 (d, i and n; column 4), and 10 mole equivalents of D_2O (e, j and o; column 5).

Discussion

The debate over the presence of nanostructured water domains in pure DES is an important issue in the field, since it is frequently inferred from *i.e.* pulsed field gradient (PFG)-NMR, which hints at differing diffusion coefficients for water in DES, and thus, this is often interpreted as a spongelike phase.[35,58–61] Our consistently flat solvent background measurements therefore show evidence that the concept similia similibus solvuntur applies to the hydrophilic ChCl : urea : water system,[62] and there is no long-range, long-timescale nanoscopic segregation of an aqueous phase, and thus no L_3 phase in the pure solvents. Any apparent separation must arise from different populations of water on the intermolecular scale, and on short time scales only,[17,58] and thus ChCl : urea does not fall in the class of DES where true nanostructure is found, or induced by water. Nanostructure in DES has been shown, but these systems tend to be actively amphiphilic, with significant hydrophobicity present,[11,37] and the ChCl : urea : water system should not be described in these terms.

The phase transitions observed on addition of AOT are shown in Fig. 5, and are intriguing, because they appear initially to give the opposite trend to those observed previously for several similar systems; for example, CnTAB micelles in ChCl : malonic acid DES contract as hydration increases, due to a hypothesized reduction in surfactant–acid interactions.[30] A reduction in the length of wormlike micelles of SDS in ChCl : U is seen as the surfactant concentration increases, but these micelles also increase in length as water content is reduced (and as ionic strength increased).[25,52]

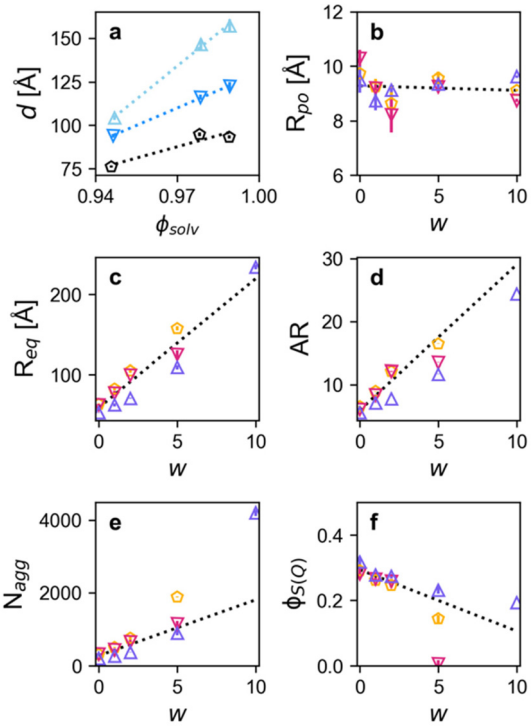

Fig. 3 *d*-Spacing from Teubner–Strey fits from varied H-AOT concentration in perdeuterated DES mixtures with $w \leq 2$ (a), plotted as a function of solvent volume fraction ($\phi_{solvent}$) demonstrating the L_3-to-L_α transition, where black pentagons are the 0*w*, blue downwards triangles are 1*w*, and light blue upwards triangles are the 2*w* DES. Fitting results are also shown from the oblate ellipsoid model (b–f); these include the polar radius R_{po} (b), equatorial radius R_{eq} (c), micelle aspect ratio (d), aggregation number (e), and hard sphere structure factor volume fraction (f), calculated for micelles as a function of solution water content, written as the DES : water mole ratio (*w*), shown as yellow pentagons (1 wt% AOT), red downwards triangles (2 wt% AOT) and purple upwards triangles (5 wt% AOT). For ellipsoid model data, parameters are weighted averages, and errors are one weighted standard deviation thereof, where the weights are used to represent the lower degree of confidence in fits to samples with poor neutron contrast, and are calculated as $\frac{(\Delta_{SLD\,i})^2}{\sum(\Delta_{SLD\,i})^2}$, summed over the three different core-solvent neutron contrasts per composition. The aspect ratio is calculated and propagated directly from the averages. The dotted lines represent linear regression fits of each dataset.

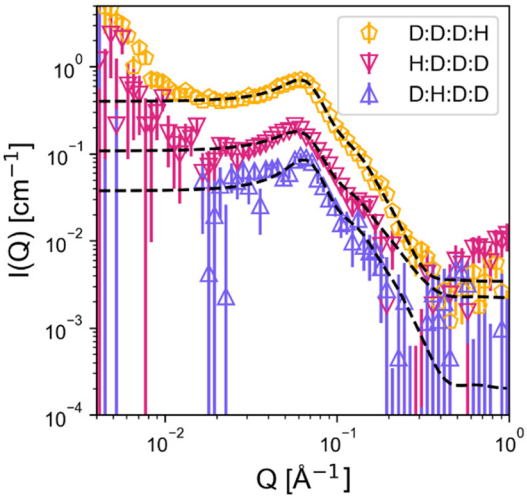

Fig. 4 SANS data and simultaneous fits to a core–shell cylinder model for the three contrasts of the anhydrous (0*w*) samples which contain 1 wt% AOT.

Here, the system contains a di-chain surfactant with a sulfonate headgroup. Ternary eutectic systems, where the urea : glycerol ratio was varied, were previously used to modulate the morphology of SDS micelles, with maximised micelle elongation correlating with smaller headgroup area, due to reduced solubility of Na^+ in the urea-rich solvent; a higher mole fraction of urea once again corresponded with maximised micelle elongation.[29] In combination with the simultaneous fitting results shown here, this offers a framework for understanding the trends observed.

In the pure (water-free) DES, an L_3 phase is formed where the micelle shell contains mostly AOT headgroups and urea, with $[cholinium]^+$ cations excluded, and Na^+ cations bound, due to low solubility of the alkali metal halide in the urea-rich DES bulk.[28,29] As water content increases, Na^+ solubility increases. Although we were not able to co-refine datasets for higher water contents, it is a reasonable assumption that, considering the significant molar excess of ChCl in the system, headgroups become increasingly solvated by choline cations, which are numerically overwhelming. The Ch^+-enrichment of the corona therefore corresponds with the expansion of the L_3 bilayer in terms of aggregation number (N_{agg}). This can be linked with Gaussian curvature elasticity; the bulky and charge-diffuse organic cation (Ch^+) has better volume matching with the AOT anions, which stabilizes the planar morphology and lamellar L_α phase,[63] as the film becomes more rigid. On the other hand, the L_3 phase is stabilised in the 'pure' low-water DES as the film has more elasticity in the presence of Na^+ cations in the micelle corona.[64] Techniques with atomistic resolution, which SANS intrinsically lacks, will be required to elucidate the exact structural picture for these ion-specific effects, since these will naturally vary depending on the nature of the adsorbed cation (*i.e.* for Na^+ relative to $[cholinium]^+$). Nevertheless, stabilisation of the reduced-curvature morphology was observed previously for aqueous AOT surfactant systems substituted with organic (imidazolium or ammonium) cations.[65,66] The unique wedgelike, di-chain, branched molecular architecture of AOT explains why the transitions observed between neighbouring phases are, in this case, L_3 and L_α, rather than transitions between for example, L_1 and L'_1 or H_1 phases.[67] However, the morphological effects remain relatable overall to the structural trends observed for surfactants such as SDS in ChCl–urea; modulation of the headgroup area and specific cation–anion volume matching allows the micelle phase to be tailored, by using the ternary DES composition to access the precise point desired on the phase diagram.[52,68]

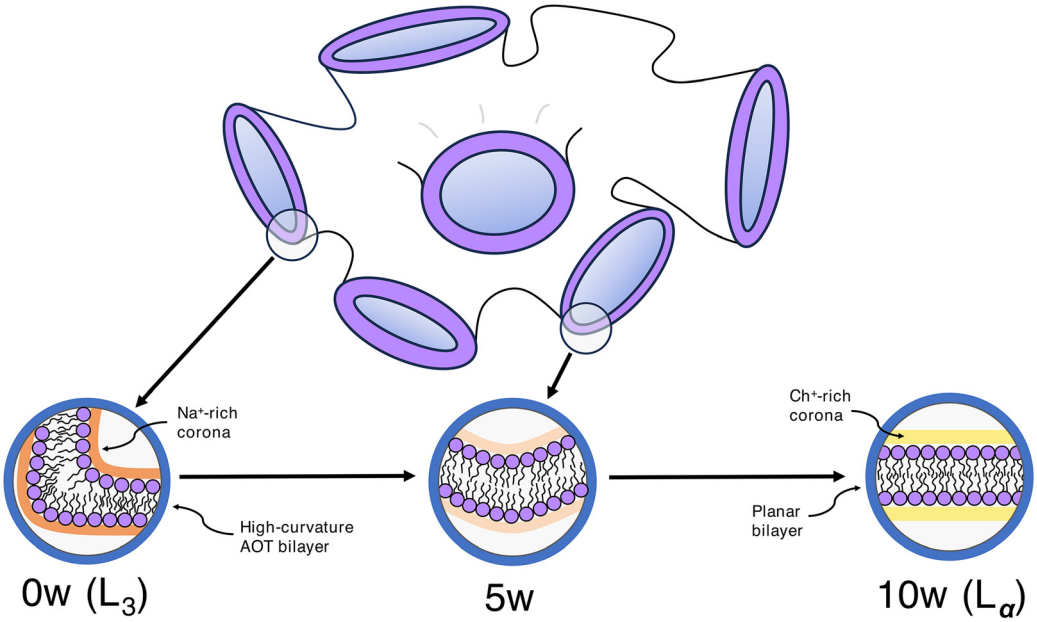

Fig. 5 Cartoon schematic of the L_3 sponge phase (top), and the local proposed structure as a function of water content shown as detailed insets (bottom).

Conclusions

The micellization of the commercially and fundamentally-relevant surfactant AOT was characterised in ternary ChCl : urea : water eutectic mixtures. First, we have shown the important result that the small-angle scattering region for these DES is flat; there is no spongelike L_3 nanostructure in the solvent itself, all water ordering is on the intermolecular scale, and all scattering signal arises from surfactant aggregates, despite suggestions of nanostructure in these hydrophilic solvent systems.

We have identified that, on addition to ChCl–urea, AOT forms a bicontinuous L_3 phase. This data can be fitted using a Teubner–Strey microemulsion model, or either an ellipsoidal (with structure factor) or lamellar model depending on the precise solvent composition. The micelle morphology has a composition-independent bilayer thickness, indicating minimal interaction between the solvent and the inner region of the micelle. We observed that the radius, aspect ratio, and aggregation number increase linearly with the DES water content, but contract at heightened surfactant concentrations.

For the pure solvents, the micelle shell is dominated by urea and AOT headgroups, with choline largely excluded. This therefore defines the behaviour in the system, which follows the same behaviour as the surfactant SDS, with differences arising due to the respective surfactant architectures. Here, Na^+ binds to surfactant headgroups at low water content because it is poorly soluble in the urea-rich solvent. As water content increases, Na^+ is substituted for $[cholinium]^+$ in the micelle shell, which alters the local Gaussian curvature due to improved cation : anion volume matching for the contact ion pairs, with both packing parameter and charge screening arguments contributing to the formation of an extensive sheet-like morphology: the transition from the L_3 to the L_α phase.

We therefore show that DES water content (*i.e.* ternary DES solvent composition) is a mechanism to tailor the size of AOT self-assembly structures and to induce transitions between neighbouring micellar phases. These results have implications for the design of biological, scientific, and industrial applications involving green 'designer' solvents and AOT, such as in nanoemulsions, nanoparticle synthesis, and extractions. While there may be no observable nanoscale DES–water segregation, the potential for controlling self-assembly processes in ionic systems, solely *via* solvent composition while using cheap, ubiquitous commercial surfactants, is perhaps even more exciting.

Author contributions

Conceptualization – OSH, KJE; Resources – PL; Formal analysis – OSH; Investigation – OSH, NSE; Visualization – OSH; Writing (original draft) – OSH; Writing (review & editing) – OSH, NSE; JD, PL, KJE; Funding acquisition – KJE.

Conflicts of interest

There are no conflicts to declare.

Acknowledgements

We thank ISIS Neutron & Muon Source for access to SANS2D under experiment number RB1610337, which can also be used

to freely access data under the ISIS-ICAT system. OSH thanks STFC (ISIS studentship agreement 3578) and the EPSRC Centre for Doctoral Training in Sustainable Chemical Technologies (EP/L016354/1); NSE also thanks the CSCT for a PhD studentship.

References

1 J. Eastoe and R. F. Tabor, *Surfactants and Nanoscience*, Elsevier B.V., 2014.
2 S. Dixit, J. Crain, W. C. K. Poon, J. L. Finney and A. K. Soper, *Nature*, 2002, **416**, 829–832.
3 M. E. Cates, D. Roux, D. Andelman, S. T. Milner and S. A. Safran, *Europhys. Lett.*, 1988, **5**, 733–739.
4 D. Anderson, H. Wennerstroem and U. Olsson, *J. Phys. Chem.*, 1989, **93**, 4243–4253.
5 H. Hoffmann, C. Thunig, U. Munkert, H. W. Meyer and W. Richter, *Langmuir*, 1992, **8**, 2629–2638.
6 R. Hayes, G. G. Warr and R. Atkin, *Chem. Rev.*, 2015, **13**, 6357–6426.
7 R. Hayes, S. Imberti, G. Warr and R. Atkin, *Phys. Chem. Chem. Phys.*, 2011, **13**, 13544–13551.
8 T. L. Greaves, D. F. Kennedy, S. T. Mudie and C. J. Drummond, *J. Phys. Chem. B*, 2010, **114**, 10022–10031.
9 T. L. Greaves and C. J. Drummond, *Chem. Soc. Rev.*, 2013, **42**, 1096–1120.
10 O. S. Hammond, R. Atri, D. T. Bowron and K. J. Edler, *Chem. – Eur. J.*, 2022, **28**, e202200566.
11 O. S. Hammond, G. Simon, M. C. Gomes and A. A. H. Padua, *J. Chem. Phys.*, 2021, **154**, 224502.
12 F. Guthrie, *London, Edinburgh Dublin Philos. Mag. J. Sci.*, 1884, **17**, 462–482.
13 L. J. B. M. Kollau, M. Vis, A. Van Den Bruinhorst, R. Tuinier and G. de With, *J. Mol. Liq.*, 2020, 9.
14 A. van den Bruinhorst and M. Costa Gomes, *Curr. Opin. Green Sustainable Chem.*, 2022, **37**, 100659.
15 O. S. Hammond, D. T. Bowron and K. J. Edler, *Green Chem.*, 2016, **18**, 2736–2744.
16 O. S. Hammond, D. T. Bowron, A. J. Jackson, T. Arnold, A. Sanchez-Fernandez, N. Tsapatsaris, V. G. Sakai and K. J. Edler, *J. Phys. Chem. B*, 2017, **121**, 7473–7483.
17 O. S. Hammond, D. T. Bowron and K. J. Edler, *Angew. Chem., Int. Ed.*, 2017, 9782–9785.
18 O. S. Hammond and K. J. Edler, *in Deep Eutectic Solvents: Synthesis, Properties, and Applications*, Wiley-VCH, Weinheim, 2019, pp. 25–42.
19 S. Kaur, M. Kumari and H. K. Kashyap, *J. Phys. Chem. B*, 2020, **124**, 10601–10616.
20 A. Sanchez-Fernandez, A. J. Jackson, S. F. Prévost, J. J. Doutch and K. J. Edler, *J. Am. Chem. Soc.*, 2021, **143**, 14158–14168.
21 M. A. Gebbie, A. M. Smith, H. A. Dobbs, A. A. Lee, G. G. Warr, X. Banquy, M. Valtiner, M. W. Rutland, J. N. Israelachvili, S. Perkin and R. Atkin, *Chem. Commun.*, 2017, **53**, 1214–1224.
22 D. A. Alonso, A. Baeza, R. Chinchilla, G. Guillena, I. M. Pastor and D. J. Ramón, *Eur. J. Org. Chem.*, 2016, 612–632.
23 J. M. Hartley, J. Allen, J. Meierl, A. Schmidt, I. Krossing and A. P. Abbott, *Electrochim. Acta*, 2022, **402**, 139560.
24 O. S. Hammond and A.-V. Mudring, *Chem. Commun.*, 2022, **58**, 3865–3892.
25 T. Arnold, A. J. Jackson, A. Sanchez-Fernandez, D. Magnone, A. E. Terry and K. J. Edler, *Langmuir*, 2015, **31**, 12894–12902.
26 A. Sanchez-Fernandez, G. L. Moody, L. C. Murfin, T. Arnold, A. J. Jackson, S. M. King, S. E. Lewis and K. J. Edler, *Soft Matter*, 2018, **14**, 5525–5536.
27 A. Sanchez-Fernandez, T. Arnold, A. J. Jackson, S. L. Fussell, R. K. Heenan, R. A. Campbell and K. J. Edler, *Phys. Chem. Chem. Phys.*, 2016, **18**, 33240–33249.
28 I. Manasi, M. R. Andalibi, R. S. Atri, J. Hooton, S. M. King and K. J. Edler, *J. Chem. Phys.*, 2021, **155**, 084902.
29 R. Atri, A. Sanchez-Fernandez, O. S. Hammond, I. Manasi, J. Doutch, J. P. Tellam and K. J. Edler, *J. Phys. Chem. B*, 2020, **124**, 6004–6014.
30 A. Sanchez-Fernandez, O. S. Hammond, A. J. Jackson, T. Arnold, J. Doutch and K. J. Edler, *Langmuir*, 2017, **33**, 14304–14314.
31 X. Meng, K. Ballerat-Busserolles, P. Husson and J.-M. Andanson, *New J. Chem.*, 2016, **40**, 4492–4499.
32 M. E. Di Pietro, O. Hammond, A. van den Bruinhorst, A. Mannu, A. Padua, A. Mele and M. Costa Gomes, *Phys. Chem. Chem. Phys.*, 2021, **23**, 107–111.
33 P. J. Smith, C. B. Arroyo, F. Lopez Hernandez and J. C. Goeltz, *J. Phys. Chem. B*, 2019, **123**, 5302–5306.
34 I. Manasi, S. J. Bryant, O. S. Hammond and K. J. Edler, in *Eutectic Solvents and Stress in Plants*, Academic Press, Cambridge MA, 2021, vol. 97, pp. 41–68.
35 C. D'Agostino, L. F. Gladden, M. D. Mantle, A. P. Abbott, E. I. Ahmed, A. Y. M. Al-Murshedi and R. C. Harris, *Phys. Chem. Chem. Phys.*, 2015, **17**, 15297–15304.
36 R. Hayes, S. Imberti, G. Warr and R. Atkin, *Phys. Chem. Chem. Phys.*, 2011, **13**, 3237–3247.
37 S. McDonald, T. Murphy, S. Imberti, G. G. Warr and R. Atkin, *J. Phys. Chem. Lett.*, 2018, **9**, 3922–3927.
38 L. N. Wong, S. Imberti, G. G. Warr and R. Atkin, *Phys. Chem. Chem. Phys.*, 2023, **25**, 31068–31076.
39 O. S. Hammond, E. K. Bathke, D. T. Bowron and K. J. Edler, *Inorg. Chem.*, 2023, **62**, 18069–18078.
40 S. Nave, J. Eastoe and J. Penfold, *Langmuir*, 2000, **16**, 8733–8740.
41 W. Philippoff and J. W. Mcbain, *Nature*, 1949, **164**, 885–885.
42 G. N. Smith, P. Brown, S. E. Rogers and J. Eastoe, *Langmuir*, 2013, **29**, 3252–3258.
43 A. K. Soper and K. J. Edler, *Biochim. Biophys. Acta, Gen. Subj.*, 2017, **1861**, 1652–1660.
44 J. K. Hensel, A. P. Carpenter, R. K. Ciszewski, B. K. Schabes, C. T. Kittredge, F. G. Moore and G. L. Richmond, *Proc. Natl. Acad. Sci. U. S. A.*, 2017, **114**, 13351–13356.

45 M. Kotlarchyk, J. S. Huang and S. H. Chen, *J. Phys. Chem.*, 1985, **89**, 4382–4386.
46 J. L. Wilson, *J. Am. Med. Assoc.*, 1955, **158**, 261.
47 Komal, G. Singh, G. Singh and T. S. Kang, *ACS Omega*, 2018, **3**, 13387–13398.
48 V. Castelletto and I. W. Hamley, *Curr. Opin. Colloid Interface Sci.*, 2002, **7**, 167–172.
49 C. P. Cabry, L. D'Andrea, N. S. Elstone, S. Kirchhecker, A. Riccobono, I. Khazal, P. Li, S. E. Rogers, D. W. Bruce and J. M. Slattery, *Phys. Chem. Chem. Phys.*, 2022, **24**, 15811–15823.
50 C. P. Cabry, L. D'Andrea, K. Shimizu, I. Grillo, P. Li, S. E. Rogers, D. W. Bruce, J. N. Canongia Lopes and J. M. Slattery, *Faraday Discuss.*, 2017, 265–289.
51 G. N. Smith and S. Prevost, *J. Appl. Crystallogr.*, 2021, **54**, 541–547.
52 A. Sanchez-Fernandez, K. J. Edler, T. Arnold, R. K. Heenan, L. Porcar, N. J. Terrill, A. Terry and A. J. Jackson, *Phys. Chem. Chem. Phys.*, 2016, **18**, 14063–14070.
53 M. Teubner and R. Strey, *J. Chem. Phys.*, 1987, **87**, 3195–3200.
54 O. S. Hammond, G. Bousrez, F. Mehler, S. Li, M. R. Shimpi, J. Doutch, L. Cavalcanti, S. Glavatskih, O. N. Antzutkin, M. W. Rutland and A.-V. Mudring, *Small*, 2023, **19**, 2300912.
55 K. M. McGrath, D. M. Dabbs, N. Yao, K. J. Edler, I. A. Aksay and S. M. Gruner, *Langmuir*, 2000, **16**, 398–406.
56 J. Marszalek, J. A. Pojman and K. A. Page, *Langmuir*, 2008, **24**, 13694–13700.
57 E. Caponetti, D. Chillura-Martino, F. Ferrante, L. Pedone, A. Ruggirello and V. Turco Liveri, *Langmuir*, 2003, **19**, 4913–4922.
58 Y. M. AlZahrani and M. M. Britton, *Phys. Chem. Chem. Phys.*, 2021, **23**, 21913–21922.
59 R. Häkkinen, O. Alshammari, V. Timmermann, C. D'Agostino and A. Abbott, *ACS Sustainable Chem. Eng.*, 2019, **7**, 15086–15092.
60 A. Abbott, L. Aldous, N. Borisenko, S. Coles, O. Fontaine, J. D. Gamarra Garcia, R. Gardas, O. Hammond, L. J. Hardwick, P.-H. Haumesser, F. Hausen, C. Horwood, J. Jacquemin, R. Jones, E. Jónsson, A. Lahiri, D. MacFarlane, G. Marlair, B. May, H. Medhi, V. H. Paschoal, J. E. S. J. Reid, T. Schoetz, K. Tamura, M. L. Thomas, S. Tiwari, B. Uralcan, A. van den Bruinhorst, M. Watanabe and J. Wishart, *Faraday Discuss.*, 2018, 405–426.
61 A. P. Abbott, S. S. M. Alabdullah, A. Y. M. Al-Murshedi and K. S. Ryder, *Faraday Discuss.*, 2017, **206**, 365–377.
62 S. Zahn, *Phys. Chem. Chem. Phys.*, 2017, **19**, 4041–4047.
63 G. Porte, J. Appell, P. Bassereau and J. Marignan, *J. Phys.*, 1989, **50**, 1335–1347.
64 M. Skouri, J. Marignan and R. May, *Colloid Polym. Sci.*, 1991, **269**, 929–937.
65 P. Brown, C. Butts, R. Dyer, J. Eastoe, I. Grillo, F. Guittard, S. Rogers and R. Heenan, *Langmuir*, 2011, **27**, 4563–4571.
66 P. Brown, C. P. Butts, J. Eastoe, D. Fermin, I. Grillo, H. Lee, D. Parker, D. Plana and R. M. Richardson, *Langmuir*, 2012, **28**, 2502–2509.
67 D. P. Bossev, S. R. Kline, J. N. Israelachvili and M. E. Paulaitis, *Langmuir*, 2001, **17**, 7728–7731.
68 A. Sanchez-Fernandez, O. S. Hammond, K. J. Edler, T. Arnold, J. Doutch, R. M. Dalgliesh, P. Li, K. Ma and A. J. Jackson, *Phys. Chem. Chem. Phys.*, 2018, **20**, 13952–13961.